Acta Pharmaceutica Sinica B 2024;14(4):1677−1692

Chinese Pharmaceutical Association
Institute of Materia Medica, Chinese Academy of Medical Sciences

Acta Pharmaceutica Sinica B

www.elsevier.com/locate/apsb
www.sciencedirect.com

ORIGINAL ARTICLE

Eubacterium coprostanoligenes alleviates chemotherapy-induced intestinal mucositis by enhancing intestinal mucus barrier

Dongsheng Bai[a,†], Jiawei Zhao[a,†], Runde Wang[a,†], Jiaying Du[a], Chen Zhou[a], Chunyang Gu[a], Yuxiang Wang[a], Lulu Zhang[b,*], Yue Zhao[a,*], Na Lu[a,*]

[a]*State Key Laboratory of Natural Medicines, Jiangsu Key Laboratory of Carcinogenesis and Intervention, Department of Physiology, School of Basic Medicine and Clinical Pharmacy, China Pharmaceutical University, Nanjing 210009, China*
[b]*Department of Clinical Pharmacology, School of Pharmacy, Nanjing Medical University, Nanjing 211166, China*

Received 3 October 2023; received in revised form 6 December 2023; accepted 25 December 2023

KEY WORDS

Chemotherapy;
Mucositis;
Eubacterium coprostanoligenes;
MUC2;
AUF1

Abstract Chemotherapy-induced mucositis represents a severe adverse outcome of cancer treatment, significantly curtailing the efficacy of these treatments and, in some cases, resulting in fatal consequences. Despite identifying intestinal epithelial cell damage as a key factor in chemotherapy-induced mucositis, the paucity of effective treatments for such damage is evident. In our study, we discovered that *Eubacterium coprostanoligenes* promotes mucin secretion by goblet cells, thereby fortifying the integrity of the intestinal mucus barrier. This enhanced barrier function serves to resist microbial invasion and subsequently reduces the inflammatory response. Importantly, this effect remains unobtrusive to the antitumor efficacy of chemotherapy drugs. Mechanistically, *E. copr* up-regulates the expression of AUF1, leading to the stabilization of *Muc2* mRNA and an increase in mucin synthesis in goblet cells. An especially significant finding is that *E. copr* activates the AhR pathway, thereby promoting the expression of AUF1. In summary, our results strongly indicate that *E. copr* enhances the intestinal mucus barrier, effectively alleviating chemotherapy-induced intestinal mucositis by activating the AhR/AUF1 pathway, consequently enhancing *Muc2* mRNA stability.

*Corresponding authors.
E-mail addresses: lulu_0219@njmu.edu.cn (Lulu Zhang), yuezhao@cpu.edu.cn (Yue Zhao), nalu@cpu.edu.cn (Na Lu).
[†]These authors made equal contributions to this work.
Peer review under the responsibility of Chinese Pharmaceutical Association and Institute of Materia Medica, Chinese Academy of Medical Sciences.

https://doi.org/10.1016/j.apsb.2023.12.015
2211-3835 © 2024 The Authors. Published by Elsevier B.V. on behalf of Chinese Pharmaceutical Association and Institute of Materia Medica, Chinese Academy of Medical Sciences. This is an open access article under the CC BY-NC-ND license (http://creativecommons.org/licenses/by-nc-nd/4.0/).

© 2024 The Authors. Published by Elsevier B.V. on behalf of Chinese Pharmaceutical Association and Institute of Materia Medica, Chinese Academy of Medical Sciences. This is an open access article under the CC BY-NC-ND license (http://creativecommons.org/licenses/by-nc-nd/4.0/).

1. Introduction

Chemotherapy-induced mucositis poses a significant adverse reaction for cancer patients undergoing treatment, characterized by painful inflammation and ulceration of the gastrointestinal mucosa[1,2]. This condition not only elicits symptoms like anorexia, vomiting, and diarrhea, but can also result in treatment delays or even cessation[3,4]. A substantial portion, approximately 40%–80%, of cancer patients undergoing chemotherapy are affected by mucositis[5]. Notably, commonly used chemotherapy drugs such as 5-fluorouracil (5FU) and irinotecan (CPT) induce severe mucositis, with about one-third of patients experiencing grade 3 or 4 diarrhea[6]. Beyond its debilitating symptoms, chemotherapy-induced mucositis significantly impairs patients' quality of life, often necessitating dose reductions, which in turn limit the effectiveness of cancer treatment and may even lead to fatal outcomes[7,8]. Presently, there is a lack of effective single interventions available for the prevention or treatment of mucositis[9]. Clinical approaches involving anti-inflammatory agents, biologic response modifiers, cytoprotective agents, antimicrobials, and antifungal agents are primarily palliative in nature, with only a few receiving approvals for use. Given the limitations of current treatments, there is an urgent need to develop effective therapies targeting mucositis[10,11].

Currently, the precise pathogenic mechanisms underlying chemotherapy-induced colitis remain elusive[12]. Intestinal mucositis involves intricate signaling pathways and processes that elicit changes in the intestinal mucosa[11]. Research investigating the relevant pathological mechanisms predominantly focuses on molecular pathways, particularly those involving intestinal epithelial cell damage and inflammatory responses[13]. However, recent studies have brought to light the significant role played by the disruption of the mucosal barrier, stemming from an imbalance in the gut microbiota, in the progression of intestinal mucositis[14]. Intestinal homeostasis relies heavily on the integrity of the mucosal barrier, composed of epithelial cells and the overlaying mucus layer, and the finely tuned dynamic balance with the gut microbiota[15]. The mucous layer in the intestine acts as a dynamic barrier, constituting the primary defense against the invasion of pathogenic microorganisms[16]. Once this mucous layer is compromised, intestinal microbes can infect the intestinal epithelial cells, subsequently triggering mucositis[17,18].

Mucins serve as the primary constituents of intestinal mucus, categorized into two types: secreted and membrane-bound mucins[19]. These molecules play a critical role in maintaining the homeostasis of the intestinal epithelium[20]. Notably, the secreted mucins, particularly MUC2 and MUC5AC, are synthesized by goblet cells and lack transmembrane domains, facilitating their extracellular secretion[21,22]. In the colon, MUC2 represents the predominant subtype of mucin[23]. Upon transcription and translation, the MUC2 precursor undergoes folding and glycosylation in the endoplasmic reticulum, leading to the formation of mature MUC2[24]. Subsequently, mature MUC2 undergoes sialylation modifications in the Golgi apparatus, resulting in the formation of large gel-like mucus, which is then stored in a specialized structure known as the goblet cell's theca[23,25]. Under the influence of intrinsic factors governing self-regulation or in response to environmental cues, MUC2 is released into the intestinal lumen in a calcium-dependent manner[26,27].

The mucous barrier formed by MUC2 plays a pivotal role in preventing intestinal bacterial invasion[28]. Recent research, however, indicates that the integrity and functionality of MUC2's mucous structure are reliant on the involvement of bacteria or their metabolites[29]. Germ-free mice, in contrast to normal mice, display a thin or locally absent colonic mucus layer, which recovers gradually upon microbial colonization[18,30]. Intestinal bacteria and their metabolites may regulate MUC2 synthesis, secretion, and glycosylation, thus influencing the formation of the intestinal mucus barrier[31]. In this study, we demonstrate that *Eubacterium coprostanoligenes* inhibits chemotherapy-induced colitis, while simultaneously promoting intestinal mucus production, without compromising tumor therapeutic efficacy. Notably, *E. copr* achieves its promotive effect on intestinal mucus synthesis by enhancing the stability of *Muc2* mRNA mediated by AUF1. Collectively, our findings suggest that *E. copr* holds promise as a valuable therapeutic strategy for chemotherapy-induced colitis.

2. Materials and methods

2.1. Reagents and antibodies

5-Fluorouracil (5FU, Cat No. HY-90006), irinotecan (CPT, Cat No. HY-16562) and CH-223191 (Cat No. HY-12684) were purchased from MCE (Med Chem Express). 5FU and CPT were dissolved in dimethyl sulfoxide (DMSO), the storing and work concentrations of the reagents used are 10 and 1 mg/mL. The AHR inhibitor CH-223191 was dissolved at 0.5% methyl cellulose (MC) and 0.5% Tween 80 in water and administered by oral gavage once a day at 10 mg/kg.

Triton X-100 was purchased from Shanghai Chao Rui Biotech. Co., Ltd. (Shanghai, China). ELISA kits for mouse IL-1β, IL-16, IL-17 and TNF-α were purchased from ABclonal Biotechnology Co., Ltd. (Wuhan, China).

Primary antibodies against mature MUC2 (ab90007) were obtained from Abcam (Cambridge, MA); antibodies against MUC2 precursor (NBP2-25221) were obtained from Novus (Centennial, USA); cleaved-caspase-3 (A11021), PCNA (A0264), AGR2 (A12411), GRP78 (A0241), CHOP (A20987), AUF1 (A23281), AhR (A1451) and β-actin (AC006) were from ABclonal Biotechnology Co., Ltd. HRP goat anti-mouse IgG (H + L; AS003) and HRP goat anti-rabbit IgG (H + L; AS014) were from ABclonal. High-sig ECL Western Blotting Substrate was from Tanon (180-5001). Alexa Fluor 488 donkey anti-rabbit IgG (A11008) and Alexa Fluor 594 donkey anti-mouse IgG (A31570) were obtained from Invitrogen. Dye DAPI was purchased from Invitrogen (Carlsbad, USA). Glycogen Periodic Acid-Schiff (PAS/Hematoxylin) Stain Kit was purchased from Solarbio Co. Ltd. (Beijing, China). Alcian Blue 8GX was purchased from Sigma–Aldrich (St. Louis, USA).

2.2. Mice

Six- to eight-week-old male BALB/c mice and C57BL/6J mice weighing 18−22 g were procured from the Shanghai Laboratory Animal Center, China Academy of Sciences. During the study, the animals were provided with ad libitum access to food and water and were kept in a 12 h light/dark cycle at a controlled temperature of 21 ± 2 °C with a relative humidity of 45 ± 10%. Laboratory animals were randomly assigned to groups of equal size. All animal samples were analyzed in a blinded manner. All animal care and experimental procedures were conducted in accordance with the guidelines approved by the University Committee on Use and Care of Animals at the China Pharmaceutical University. The animal studies are reported in accordance with the ARRIVE guidelines.

2.3. Mouse intervention study with E. copr

E. copr (ATCC 51222) was procured from the American Type Culture Collection (ATCC) and stored in a −80 °C with 10% glycerol. Cultures were cultivated anaerobically using sterile Trypticase soy agar/broth supplemented with defibrinated sheep blood. For *E. copr* collection during the logarithmic growth phase, cultures were diluted to 5×10^6 colony-forming units per milliliter in sterile phosphate buffer solution (PBS).

C57BL/6 mice were randomly assigned to three groups: the normal group, CPT/5FU group, and CPT/5FU+*E.copr* group, with six mice in each group. In addition to the normal group, 5-fluorouracil (25 mg/kg/day) and irinotecan (25 mg/kg/day) were administered intraperitoneally from Day 0 to Day 4. Subsequently, mice in the CPT/5FU+*E.copr* group were orally gavaged with live *E. copr* (0.2 mL/10 g) daily from Day 0 to Day 9.

For the tumor-bearing model, HCT116 cells (2×10^6) were inoculated in the right flank of BALB/c mice. Mice with a tumor volume of 50 mm^3 were divided into three groups ($n = 6$ per group). Tumor largest diameter (a) and perpendicular (b) of the tumor were measured and tumor volume was calculated (volume $= a \times b^2/2$). After sacrificing the mice on Day 9, solid tumors were separated.

2.4. Immunohistochemistry

Staining was performed as previously reported. The sections were blocked with 3% goat serum, and incubated with primary antibodies for 4 h at room temperature. The sections were then detected using DAB. Images were acquired, and the optical or fluorescence intensity was evaluated by ImageJ software (National Institutes of Health, USA).

2.5. Immunofluorescence

Fixed cells were prepared for confocal imaging by fixing them with 4% paraformaldehyde in PBS, permeabilizing them with 0.5% Triton X-100, and blocking them with 3% BSA for 1 h. The samples were incubated overnight at 4 °C with primary antibodies diluted 1:100. The samples were incubated overnight at 4 °C with primary antibodies diluted 1:100. Subsequently, the cells were washed three times with PBS and stained with DAPI. Finally, the slides were imaged using a confocal laser scanning microscope (Fluoview™ FV3000, Olympus, Japan).

2.6. Hematoxylin and Eosin staining

Paraffin-embedded colon sections were respectively deparaffinized and stained with Hematoxylin and Eosin.

2.7. Alcian blue staining

Alcian blue staining was performed by the following protocol: initial deparaffinization and hydration were carried out in distilled water, followed by a 30 min immersion in an Alcian blue solution. Subsequently, a 2 min tap water wash was followed by Hematoxylin staining. Distilled water was used for further rinsing. Dehydration encompassed two rounds of 95% ethanol and two rounds of anhydrous ethanol, each step lasting 3 min. This was succeeded by three 3 min treatments with xylene. Final covering with a coverslip.

2.8. Periodic acid Schiff staining

PAS staining was performed by the following protocol: initial deparaffinization and hydration were carried out in distilled water, followed by a 20 min immersion in a Schiff Reagent solution. Subsequently, a 2 min tap water wash was followed by Hematoxylin staining. Distilled water was used for further rinsing. Dehydration encompassed two rounds of 95% ethanol and two rounds of anhydrous ethanol, each step lasting 3 min. This was succeeded by three 3 min treatments with xylene. Final covering with a coverslip.

2.9. Cytokine quantification by enzyme-linked immunoassay

Colons from mice in each group were homogenate with lysis buffer to extract total protein. The homogenate was centrifuged at 12,000×g at 4 °C for 15 min. The amount of total extracted protein was determined by BCA protein assay kit (Thermo, MA, USA). IL-1β, IL-16, TNF-α and IL-17 production in the mice serum were measured by ELISA kits according to the manufacturers' recommendations.

2.10. RNA isolation and qPCR

RNA was isolated from colons and reverse transcribed, and qPCR was performed as previously described[32]. Primer sequences are as follows:

Mouse *Il1b*-sense (5′-CCAAGCTTCCTTGTGCAAGTA-3′);
Mouse *Il1b*-antisense (5′-AAGCCCAAAGTCCATCAGTGG-3′);
Mouse *Il6*-sense (5′-ACAACCACGGCCTTCCCTAC-3′);
Mouse *Il6*-antisense (5′-TCTCATTTCCACGATTTCCCAG-3′);
Mouse *Tnfa*-sense (5′-ATGAGCACAGAAAGCATGATCCGC-3′);
Mouse *Tnfa*-antisense (5′-AAAGTAGACCTGCCCGGACTC-3′);
Mouse *Il17*-sense (5′-TCAGCGTGTCCAAACACTGAG-3′);
Mouse *Il17*-antisense (5′-CGCCAAGGGAGTTAAAGACTT-3′);
Mouse *18s*-sense (5′-CGATCCCAGGGCCTCACTA-3′);
Mouse *18s*-antisense (5′-AGTCCCTGCCCTTTGTACACA-3′);
Human *Muc2*-sense (5′-AACACAGTCCTGGTGGAAGG-3′);
Human *Muc2*-antisense (5′-CATTGTCAGGTCCCACACAG-3′);
Human *Muc5ac*-sense (5′-TCAGCACCAGTGCCCAAGTC-3′);
Human *Muc5ac*-antisense (5′-GTTGCAGGCGCAGCTGTACT-3′);
Human *Math1* sense (5′-GCTGGACGCTCTGCACTTCT-3′);
Human *Math1*-antisense (5′-CTTGCCTCATCCGAGTCACTG TAA-3′);
Human *Hes1*-sense (5′-TGGAGAGGCGGCTAAGGTGTT-3′);
Human *Hes1*-antisense (5′-TGGAAGGTGACACTGCGTTGG-3′);

Human *Auf1*-sense (5′-GATCAAGGGGTTTTGGCTTT-3′);
Human *Auf1*-antisense (5′-GTTGTCCATGGGGACCTCT-3′);
Human *Gadph*-sense (5′-AAGATCATCAGCAATGCCTCCT GC-3′);
Human *Gadph*-antisense (5′-ATGGACTGTGGTCATGAGTC CTTC-3′).

2.11. Western blot analysis

Proteins were extracted by incubating the cell pellet or tissue in RIPA buffer containing 1% PMSF and 1% phosphatase inhibitors. Protein concentration was quantified using a BCA protein quantification kit. The proteins were separated using sodium dodecyl sulfate-polyacrylamide gel electrophoresis (SDS-PAGE) and subsequently transferred to a nitrocellulose membrane. Following a 1 h blocking step at room temperature with 5% BSA, the membrane was then incubated with primary antibodies overnight at 4 °C. The membrane was washed with PBST, incubated with horseradish peroxidase (HRP)-labeled secondary antibodies at room temperature for 1 h, and then exposed to the ECL reagent.

2.12. Cell culture

HCT116, HT29 and LS174T (human colon cancer) were obtained from American Type Culture Collection (ATCC). The cells were cultured with DMEM medium (Gibco, Carlsbad, USA) supplemented with 10% (*v*/*v*) fetal bovine serum (Gibco, Carlsbad, USA), 100 U/mL benzyl penicillin and 100 mg/mL streptomycin. Cells were cultured in a humidified environment with 5% CO_2 at 37 °C.

2.13. Organoid culture

Small intestines were opened longitudinally, cut into 0.2 cm pieces, and washed with ice-cold PBS. Intestinal crypts were isolated by treatment with EDTA and then passed through a 70 μm cell strainer. Equal numbers of isolated crypts were mixed 1:1 (*v*/*v*) with Matrigel (Cat: 356231, Corning, USA) and plated in 48-well plates. Matrigel was polymerized by incubating it at 37 °C for 15 min, and 400 μL of DMEM/F-12 (Cat: 12500096, GIBCO, USA) with cytokines (R&D Systems, USA) were added into each well[33]. The culture medium was replaced every 3 days and the organoids were passaged by mechanical dissociation every 7 days.

2.14. Cell viability assay

The CCK-8 reagent (Beyotime, Shanghai, China) was used for detection according to the user's manual. A 10 μL solution of CCK-8 was added to cells seeded in a 96-well plate. The cells were harvested at the indicated time points, and the cell proliferation was quantified after a 2 h incubation period and was determined by measuring the OD_{450}.

2.15. RNA immunoprecipitation (RIP) assay

When cells reached 80% confluence, LS174T cells were infected with *E. copr* for 12 h and cultured for another 24 h before lysis. Cells infected with or without *E. copr* were collected and the subsequent RIP assay was performed according to the manual of the RIP kit (Geneseed Biotech Co., Cat. No. P0101). Anti-AUF1 (50 μg) was added to precipitate RNA−protein complex. Anti-rabbit IgG (50 μg) was used as control. The RNA isolated from all groups was used to perform real-time PCR.

2.16. Luciferase reporter assay

The pGL3 plasmid and pRL-TK plasmid were transfected into cells using Lipofectamine 2000 reagent. Then cells were assayed by using a Dual Luciferase Reporter Assay Kit (Vazyme, Nanjing, China). Luciferase intensity was detected with a Luminoskan Ascent (Thermo Fisher Scientific Inc., Finland).

2.17. Chromatin immunoprecipitation (ChIP) assay

Cells were cross-linked with 1% formaldehyde, quenched with 125 mmol/L glycine, washed with PBS, sonicated with Covaris M220 ultrasonicator (Covaris, MA, USA) and centrifuged at 4 °C. DNA was fragmented into around 250 bp. Protein A/G magnetic beads were preincubated with IgG or AhR antibody at 4 °C overnight. Cell lysates were then incubated with pretreated Protein A/G magnetic beads at 4 °C for 4 h. Finally, immune complexes were eluted with elution buffer (1% SDS, 0.1 mol/L $NaHCO_3$, pH 8.4) at room temperature for 10 min. Reverse cross-linking was performed at 65 °C overnight in a high salt buffer (0.2 mol/L NaCl, 50 mmol/L Tris, pH 6.5, 10 mmol/L EDTA, 0.2 mg/mL proteinase K [Beyotime, ST532]). Extracted and purified immune-precipitated DNA was quantified by real-time PCR.

2.18. Statistical analysis

The data shown in the study were obtained in at least three independent experiments and all results represent the mean ± SD. Differences between the groups were assessed by one-way ANOVA test. Details of each statistical analysis used are provided in the figure legends. Differences with P values < 0.05 were considered statistically significant.

3. Results

3.1. E. copr exhibits no impact on the anti-colorectal cancer effects of CPT and 5FU

To assess the potential influence of *E. copr* on CPT and 5FU chemotherapy efficacy, we established an HCT116 colorectal cancer xenograft model. Analysis of tumor volume demonstrated that both CPT and 5FU treatments significantly suppressed tumor growth, whereas *E. copr* had no effect on the anti-tumor activity of these drugs (Fig. 1A). Visually, tumors treated with CPT and 5FU appeared smaller, while no significant changes in tumor size were observed following *E. copr* treatment (Fig. 1B). Furthermore, the tumor weight of mice treated with CPT and 5FU was significantly lower compared to the control group, whereas no change in tumor weight occurred after *E. copr* treatment (Fig. 1C). Assessment of proliferating cell nuclear antigen (PCNA) staining in tumor tissues of each group revealed significant inhibition of tumor cell proliferation after CPT and 5FU treatment, with no effect on tumor tissue proliferation observed with *E. copr* treatment (Fig. 1D). Additionally, examination of cleaved-Caspase 3 levels in tumor tissues showed a notable enhancement of apoptosis in response to CPT and 5FU treatment, while *E. copr* had no impact on tumor cell apoptosis (Fig. 1E). Similar results were obtained from TUNEL staining analysis (Fig. 1F). To investigate the effect of *E. copr* on the growth of colorectal tumors at the primary site, orthotopic xenografts of HCT116 cells were established. Our results revealed that the treatment of CPT and 5FU effectively inhibited the growth of orthotopic transplantation colorectal

tumors. Importantly, *E. copr* did not exert any discernible influence on the therapeutic efficacy of CPT and 5FU (Fig. 1G). Collectively, these findings indicate that *E. copr* does not influence the anti-colorectal cancer effects of CPT and 5FU.

3.2. *E. copr alleviates intestinal mucositis induced by CPT and 5FU in tumor-bearing mice*

In the process of investigating the anti-colon cancer effects of *E. copr* on CPT and 5FU, we recorded the changes in body weight of tumor-bearing mice. Exposure to CPT and 5FU resulted in a significant reduction in the mice's body weight. However, when compared to the groups treated with CPT and 5FU, the tumor-bearing mice treated with *E. copr* showed a notable improvement in body weight reduction (Fig. 2A). Furthermore, it was observed that treatment with CPT and 5FU led to a considerable shortening of the colon. However, *E. copr* effectively mitigated the colon shortening induced by CPT and 5FU (Fig. 2B and C). For an assessment of tissue damage in the colon among different groups, histological examination using H&E staining was performed. The mice treated with CPT and 5FU exhibited severe mucosal structural damage with extensive infiltration of inflammatory cells, while the mice treated with *E. copr* showed reduced tissue damage (Fig. 2D). Additionally, treatment of CPT and 5FU induced significant apoptosis in colon tissues, whereas treatment of *E. copr* did not impact colon tissue apoptosis (Fig. 2E and F). Taken together, these results strongly suggest that *E. copr* effectively ameliorates colon injury caused by CPT and 5FU in tumor-bearing mice.

3.3. *E. copr attenuates CPT and 5FU induced intestinal mucositis in C57BL/6J mice*

A chemotherapy-induced colitis model was established in C57BL/6J mice. Our observations indicate that exposure to CPT and 5FU significantly reduced the body weight of the mice. However, *E. copr* effectively ameliorated the weight loss induced by these chemotherapeutic agents (Fig. 3A). Additionally, we found that *E. copr* treatment suppressed colon shortening caused by CPT and 5FU (Fig. 3B and C). Similarly, CPT and 5FU promoted colonic tissue damage in C57BL/6J mice, which was mitigated by *E. copr* (Fig. 3D). However, it is worth noting that *E. copr* did not affect colonic tissue apoptosis (Fig. 3E and F). Moreover, treatment of CPT and 5FU significantly increased the secretion of IL-1β, IL-6, IL-17, and TNF-α in serum of C57BL/6J mice. Interestingly, these elevated cytokine levels were effectively reversed by *E. copr* (Fig. 3G). Similar results were observed when measuring the mRNA levels of pro-inflammatory cytokines in colonic tissue (Fig. 3H). Overall, these findings collectively demonstrate that *E. copr* markedly alleviates chemotherapy-induced colitis.

3.4. *E. copr alleviates mucin loss induced by CPT and 5FU*

Chemotherapy-induced colitis arises primarily from the damage inflicted upon intestinal epithelial cells by chemotherapy drugs[34]. The mucous layer produced by goblet cells, a type of epithelial cell, plays a pivotal role in protecting against intestinal microbial invasion[35]. To assess the impact of *E. copr* on mucous layer, we utilized Alcian blue and periodic acid-Schiff (PAS) staining to observe the mucous layer and mucin-producing goblet cells in mice following exposure to CPT and 5FU. Our findings revealed a reduction in the mucous layer and depletion of goblet cells in the colon under chemotherapy exposure. However, upon *E. copr* treatment, significant restoration of the mucous layer and goblet cell depletion was observed in mice (Fig. 4A and B). Immunofluorescence staining of mouse colon tissue using MUC2 antibodies demonstrated a decrease in MUC2-positive goblet cells after CPT and 5FU exposure, while *E. copr* treatment led to a substantial increase in MUC2-positive goblet cells (Fig. 4C). Furthermore, we assessed the levels of mature MUC2 protein in colon tissue. Compared to normal mice, the levels of mature MUC2 protein were significantly reduced in mice treated with CPT and 5FU at 3, 6, and 9 days. However, *E. copr* treatment for 6 and 9 days restored MUC2 expression (Fig. 4D). In addition, we examined the expression of tight junction-related proteins, Claudin-1 and ZO-1, in colon tissue. Exposure to CPT and 5FU resulted in a significant decrease in the expression of Claudin-1 and ZO-1. However, *E. copr* treatment had no effect on the expression of these proteins in colon tissue (Fig. 4E and F). Taken together, these findings indicate that *E. copr* alleviates CPT and 5FU-induced reduction of mature MUC2, without affecting the tight junctions of intestinal epithelial cells.

3.5. *E. copr enhances MUC2 mRNA expression in goblet cells*

The translation of the MUC2 precursor requires folding and glycosylation within the endoplasmic reticulum (ER) to form mature MUC2[36]. To investigate the mechanism by which *E. copr* restores the chemotherapy-induced reduction of mature MUC2, we examined the expressions of mature MUC2, MUC2 precursor, and ER stress-related proteins. Exposure to CPT and 5FU significantly decreased the protein expression of both mature MUC2 and MUC2 precursors in colon tissues, but this effect was reversed by *E. copr*. However, the expression of ER stress-related proteins remained unchanged throughout this process (Fig. 5A). Likewise, *E. copr* infection increased the protein expression of both mature MUC2 and MUC2 precursor in goblet cells, without affecting the expression of ER stress-related proteins (Fig. 5B). This finding was further confirmed by immunofluorescence staining (Fig. 5C). These results suggest that *E. copr* does not impact the maturation process of MUC2 in the ER. In order to understand the effect of *E. copr* on intestinal epithelial cells, we utilized the *ex vivo* organoid culture model to study associated phenotypes after *E. copr* treatment. The formation of intestinal organoids begins with intestinal crypts composed of ISCs[37]. These cells are located in the crypt region and give rise to progenitor cells that subsequently differentiate into the specialized IECs of the villi[38]. We found a significant increase in MUC2 expression after *E. copr* treatment during the cystic formation stage of the organoid (Fig. 5D). Furthermore, *E. copr* did not affect organoid budding (Fig. 5E).

Given the upregulation of MUC2 precursor expression by *E. copr*, we investigated its effect on *Muc2* mRNA expression in goblet cells. Firstly, we observed that different levels of *E. copr* infection did not affect the viability of goblet cells (Fig. 5F). In contrast, *E. copr* significantly increased *Muc2* mRNA levels in goblet cells, but did not affect *Muc5ac*, *Math1* and *Hes1* mRNA levels (Fig. 5G). We also found that *E. copr* similarly increased *Muc2* mRNA levels in colon tissue (Fig. 5H). Moreover, with the increase of *E. copr* infection, the *Muc2* mRNA level also increased accordingly, whereas *Muc5ac* mRNA level remained unaffected. At the same time, infection with *E. coli* did not show a similar effect on *Muc2* mRNA level (Fig. 5I and J). Correspondingly, *E. copr* increased *Muc2* mRNA level in a time-dependent manner, without affecting

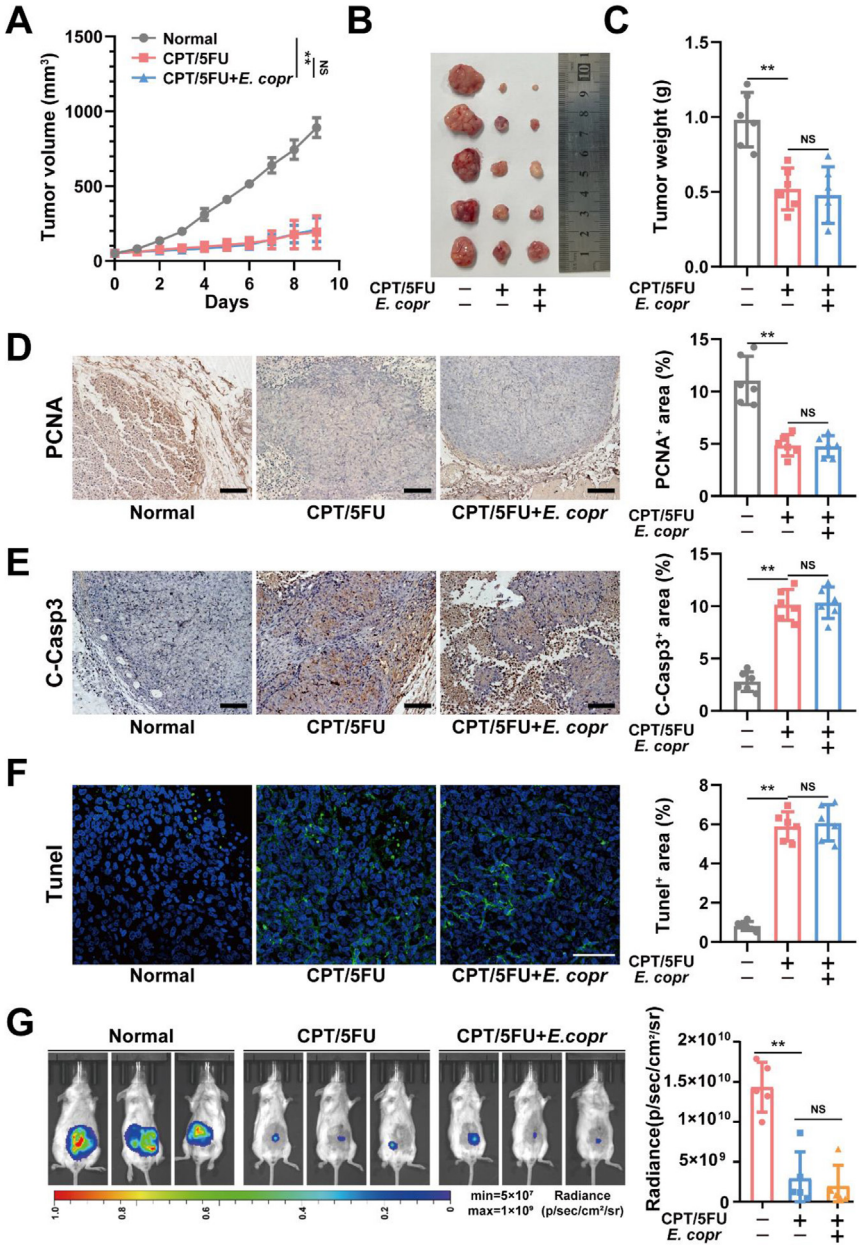

Figure 1 *E. copr* did not affect the tumor inhibitory effect of CPT/5FU *in vivo*. (A) Tumor volume in the control, CPT/5FU and *E. copr* groups were recorded daily. (B) Tumors images were obtained from indicated group on Day 9. (C) Weight of tumors were measured from indicated group. Expression of PCNA (D) and Cleaved-Caspase 3 (C-Casp3) (E) was measured by IHC and quantified by ImageJ in the tumor sections. Scale bar: 100 μm. (F) TUNEL staining and the quantification of TUNEL-positive cell was performed in tumor tissues. Scale bar: 20 μm. (G) Bioluminescence was detected and quantified in orthotopic xenografts of luciferase-labeled HCT116 cells from indicated group. The values are expressed as the mean ± SD, $^{**}P < 0.01$. NS, not significant.

Muc5ac. Similarly, no similar effect was observed with *E. coli* infection (Fig. 5K and L). These findings demonstrate that *E. copr* specifically increases the mRNA level of *Muc2* in goblet cells.

3.6. *E. copr stabilizes Muc2 mRNA via AUF1*

To elucidate the molecular mechanism underlying the upregulation of *Muc2* mRNA by *E. copr*, we assessed the stability of *Muc2* mRNA using actinomycin D to block *de novo* transcription. Remarkably, we observed that *E. copr* prolonged the half-life of *Muc2* mRNA without impacting *Muc5ac* mRNA half-life (Fig. 6A). Subsequently, we focused on post-transcriptional mechanisms regulating *Muc2*, which involve RNA-binding proteins (RBPs). Employing RNA sequencing (RNA-seq) in conjunction with gene set enrichment analysis (GSEA), we observed a significant enrichment of AUF1-bound mRNAs upon *E. copr* infection, strongly implicating AUF1 in the stabilization of *Muc2* mRNA (Fig. 6B). Both Western blot and qPCR results

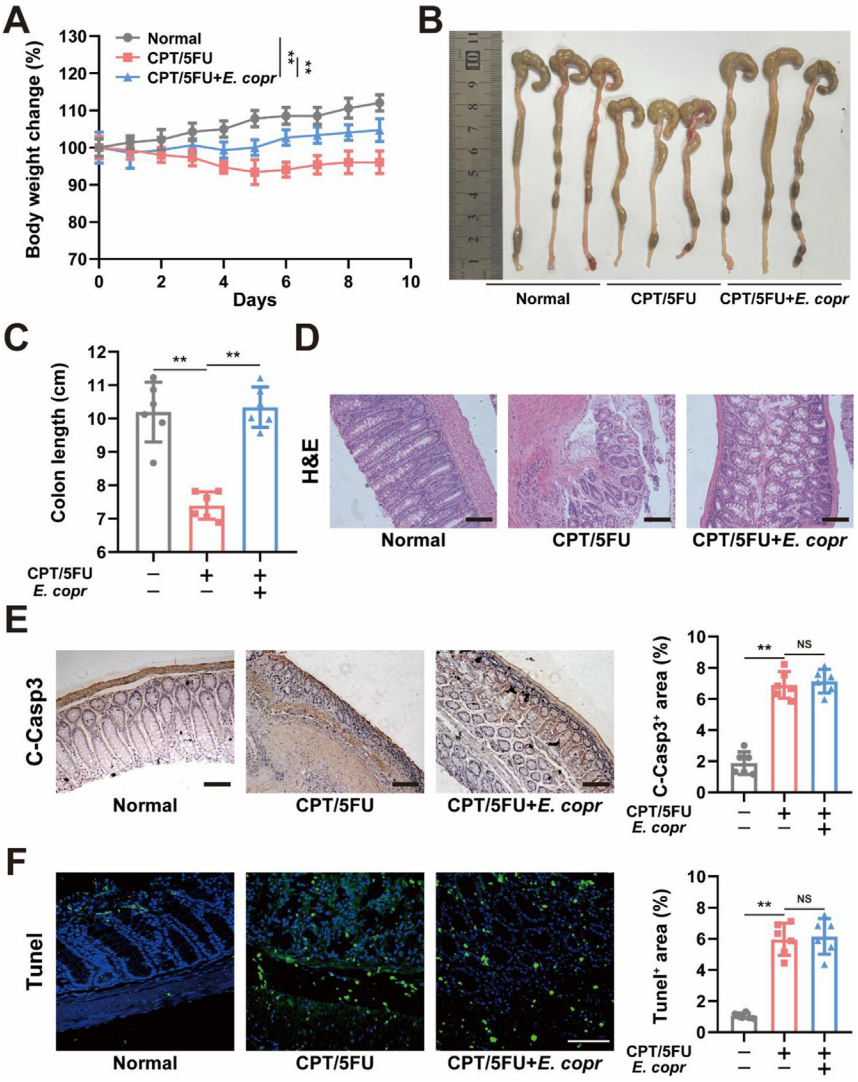

Figure 2 *E. copr* prevented intestinal mucositis induced by CPT/5FU in tumor-bearing mice. (A) Body weight of tumor-bearing mice in the control, CPT/5FU and *E. copr* groups were recorded daily. (B) Colon images of tumor-bearing mice in the indicated group were obtained on Day 9. (C) The colon length was measured from indicated group tumor-bearing mice. (D) Representative images of the histopathology of the colon sections were obtained from indicated group. Scale bar: 100 μm. (E) Expression of Cleaved-Caspase 3 (C-Casp3) was measured by IHC and quantified by ImageJ in the colon sections. Scale bar: 100 μm. (F) TUNEL staining and the quantification of TUNEL-positive cell was performed in the colon sections. Scale bar: 20 μm. The values are expressed as the mean ± SD, $^{**}P < 0.01$. NS, not significant.

confirmed that the levels of *Auf1* protein and mRNA increase in response to *E. copr* infection (Fig. 6C). In addition, *E. copr* increased *Auf1* protein and mRNA levels in colon tissue (Fig. 6D). Further, using RNA immunoprecipitation (RIP), a method to identify specific mRNA binding to known proteins, we discovered direct binding of AUF1 protein to *Muc2* mRNA compared to the negative control (GAPDH). Moreover, in goblet cells infected with *E. copr*, the mRNA level of *Muc2* increased, likely attributed to the elevated expression of AUF1 protein upon *E. copr* infection (Fig. 6E). AUF1 has been previously shown to bind to adenine-uridine-rich elements (AREs) and regulate the stability of ARE-mRNAs[39,40]. The 3′ untranslated region (3′UTR) of *Muc2* was identified to contain an ARE site. To investigate its functional role, we employed pGL3-luciferase reporter vectors encoding the *Muc2* 3′UTR intact region or fragments that contain or do not contain the ARE site (Fig. 6F). Upon transfection with the pGL3 vector containing the ARE region of *Muc2* 3′UTR, *E. copr* significantly increased luciferase activity. In contrast, *E. copr* had no effect on luciferase activity in cells transfected with the pGL3 vector containing the non-ARE region of *Muc2* 3′UTR (Fig. 6F). Subsequently, we introduced mutations into the ARE region of *Muc2* 3′UTR and found that *E. copr* significantly increased luciferase activity in cells containing the wild-type *Muc2* 3′UTR. Conversely, *E. copr* had no effect on luciferase activity in cells containing the mutant *Muc2* 3′UTR (Fig. 6G).

Following the identification of potential AUF1 binding sites on the *Muc2* 3′UTR, we investigated whether AUF1 is involved in the stabilization of *Muc2* mRNA by *E. copr*. Knockdown of AUF1 in

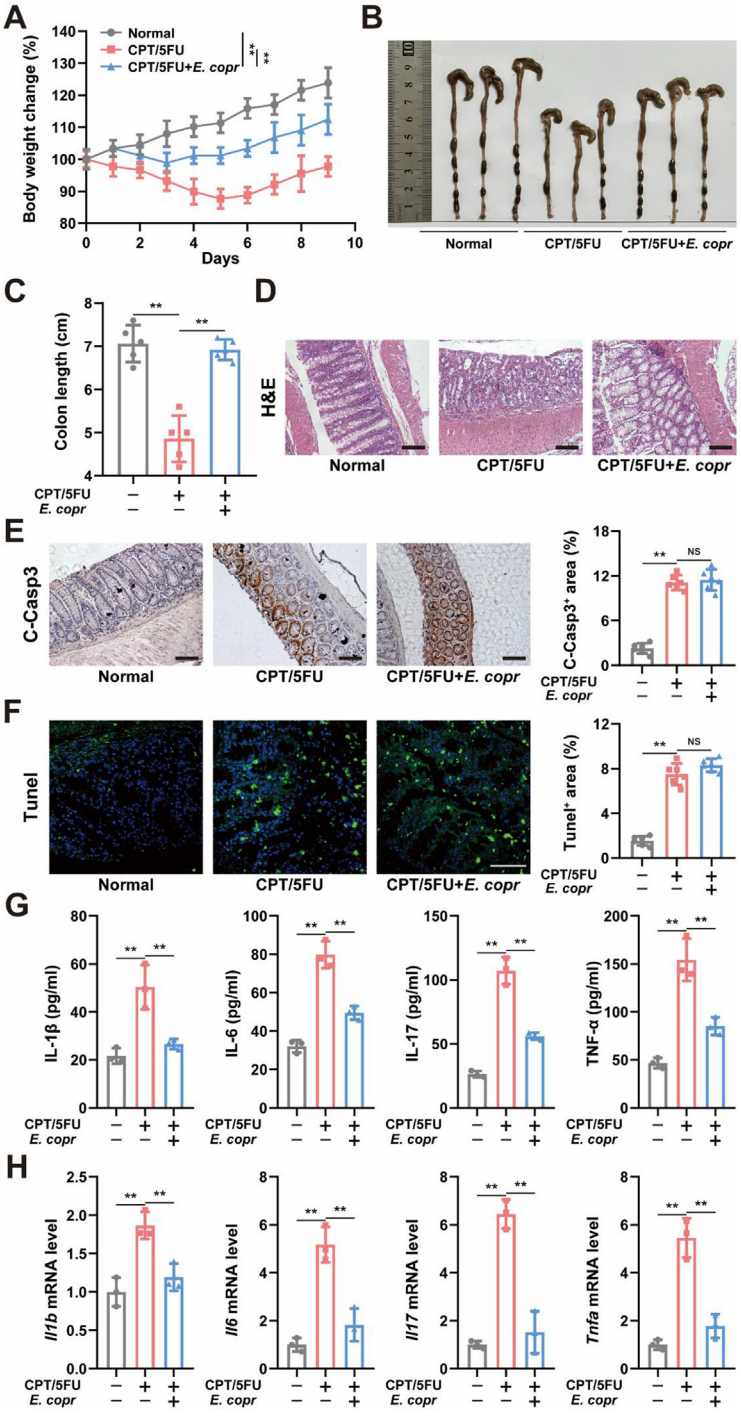

Figure 3 *E. copr* ameliorated intestinal mucositis induced by CPT/5FU. (A) Body weight in the control, CPT/5FU and *E. copr* groups were recorded daily. (B) Images of the colon in the indicated group were obtained on Day 9. (C) The colon length was measured in the indicated. (D) Representative images of the histopathology of the colon sections were obtained from indicated group. Scale bar: 100 μm. (E) Expression of Cleaved-Caspase 3 (C-Casp3) was measured by IHC and quantified by ImageJ in the colon sections. Scale bar: 100 μm. (F) TUNEL staining and the quantification of TUNEL-positive cell was performed in the colon sections. Scale bar: 20 μm. (G) Serum levels of IL-1β, IL-6, IL-17 and TNF-α were measured in the indicated group mice. (H) The mRNA levels of *Il1b*, *Il6*, *Il17* and *Tnfa* were measured in the colon tissues of indicated group mice. The values are expressed as the mean ± SD, $^{**}P < 0.01$. NS, not significant.

goblet cells resulted in a significantly shorter half-life of *Muc2* mRNA (Fig. 6H and I). Furthermore, the upregulation of *Muc2* protein and mRNA expression by *E. copr* was abolished in AUF1 knockdown cells (Fig. 6J and K). These results provide strong evidence supporting the role of AUF1 in *E. copr*-mediated stabilization of *Muc2* mRNA.

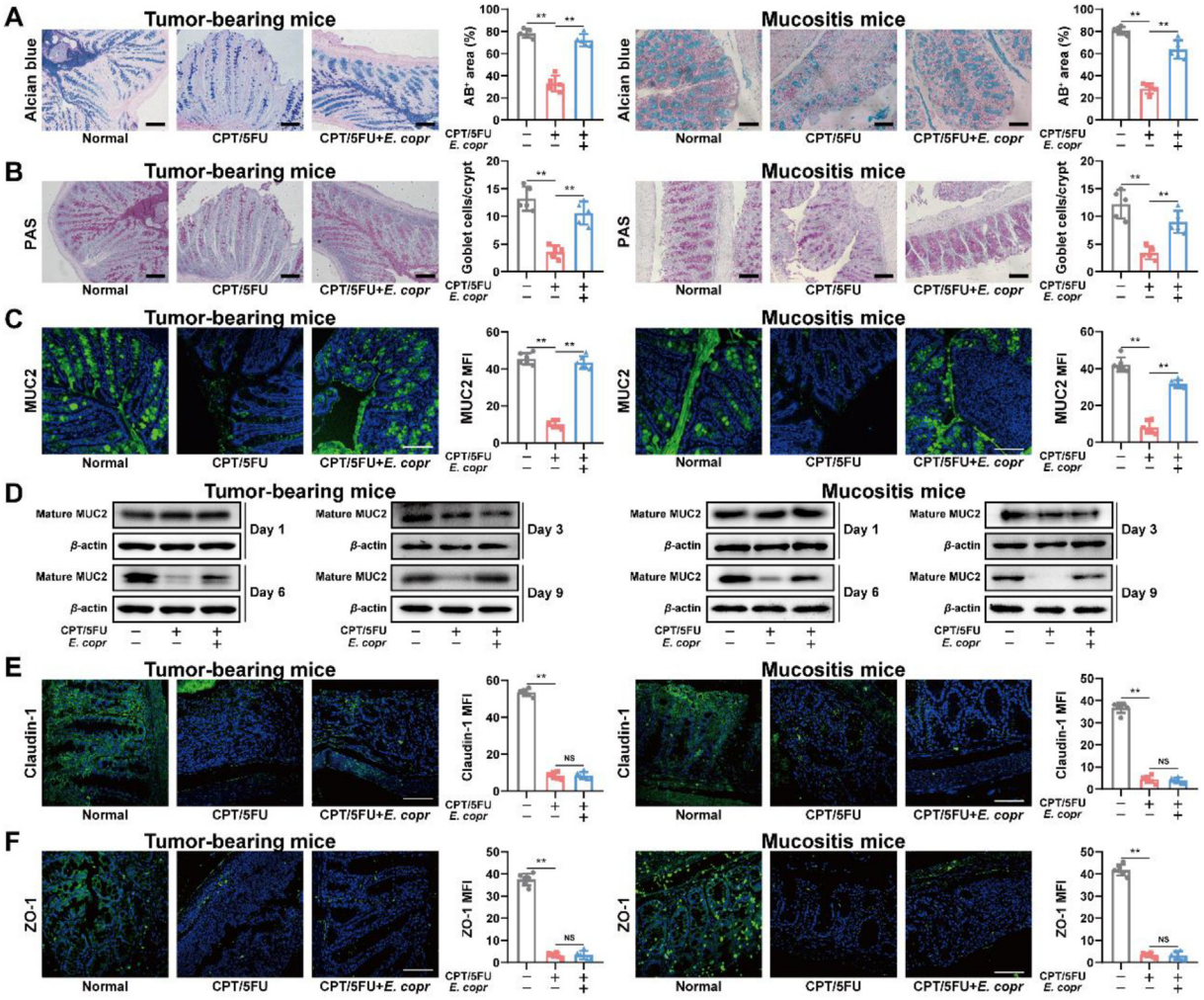

Figure 4 *E. copr* alleviated loss of the mucous layer induced by CPT/5FU. Alcian blue (A) and periodic acid-Schiff (B) were performed in colon sections from tumor-bearing mice and mucositis mice. Scale bar: 100 μm. (C) Expression of MUC2 was analyzed in colon sections from tumor-bearing mice and mucositis mice by immunofluorescence staining. Scale bar: 20 μm. (D) Expression of colonic mature MUC2 in indicated time was analyzed from tumor-bearing mice and mucositis mice. Claudin-1 (E) and ZO-1 (F) immunofluorescence staining were performed in colon sections from tumor-bearing mice and mucositis mice. Scale bar: 20 μm. The values are expressed as the mean ± SD, $^{**}P < 0.01$. NS, not significant.

3.7. E. copr promotes AUF1 transcription and enhances Muc2 mRNA stability through AhR activation

The qPCR results revealed a significant increase in *Auf1* mRNA levels upon *E. copr* infection. Subsequently, the upregulation of *Auf1* mRNA levels in response to *E. copr* was completely reversed upon treatment with actinomycin D (Fig. 7A). This suggests that the *E. copr*-mediated upregulation of *Auf1* mRNA occurs at the transcriptional level.

Using the HOMER (Hypergeometric Optimization of Motif Enrichment) algorithm, we identified the top ten significantly enriched transcription factor (TF) binding motifs in the promoters of the upregulated *Auf1* (Fig. 7B). Furthermore, the GSEA revealed a positive enrichment of genes regulated by Aryl Hydrocarbon Receptor (AhR) in these TFs upon *E. copr* infection (Fig. 7C). Moreover, the mRNA levels of *Cyp1a1* and *Cyp1b1* were obviously increased after infection of *E. copr* (Fig. 7D). This indicates that AhR was significantly activated by infection of *E. copr*. Consequently, it is inferred that *E. copr* may promote *Auf1* transcription by activating AhR. To identify the specific elements responsible for *E. copr* in the *Auf1* promoter, we constructed various 5′ deletions of the *Auf1* promoter. Our experiments indicated that the region from nucleotide −750 to −100 contains putative *E. copr*-responsive regulatory elements (Fig. 7E). By comparing the *Auf1* promoter in the JASPAR database, we discovered the presence of four AhR elements in the region from −750 to −100. Consequently, we generated mutant variants for each of these four AhR elements (Fig. 7F). Results confirmed that the region from −122 to −112 nucleotides is the *E. copr*-mediated AhR element (Fig. 7G). To confirm the binding of AhR to the *Auf1* promoter, chromatin immunoprecipitation (ChIP) experiments were performed, and the results demonstrated a direct binding of AhR to the region from nucleotide −122 to −112 of the *Auf1* promoter (Fig. 7H). To better understand how *E. copr* regulates *Auf1*, we determined that *E. copr* significantly increases RNA polymerase II binding to the *Auf1* promoter. The interaction

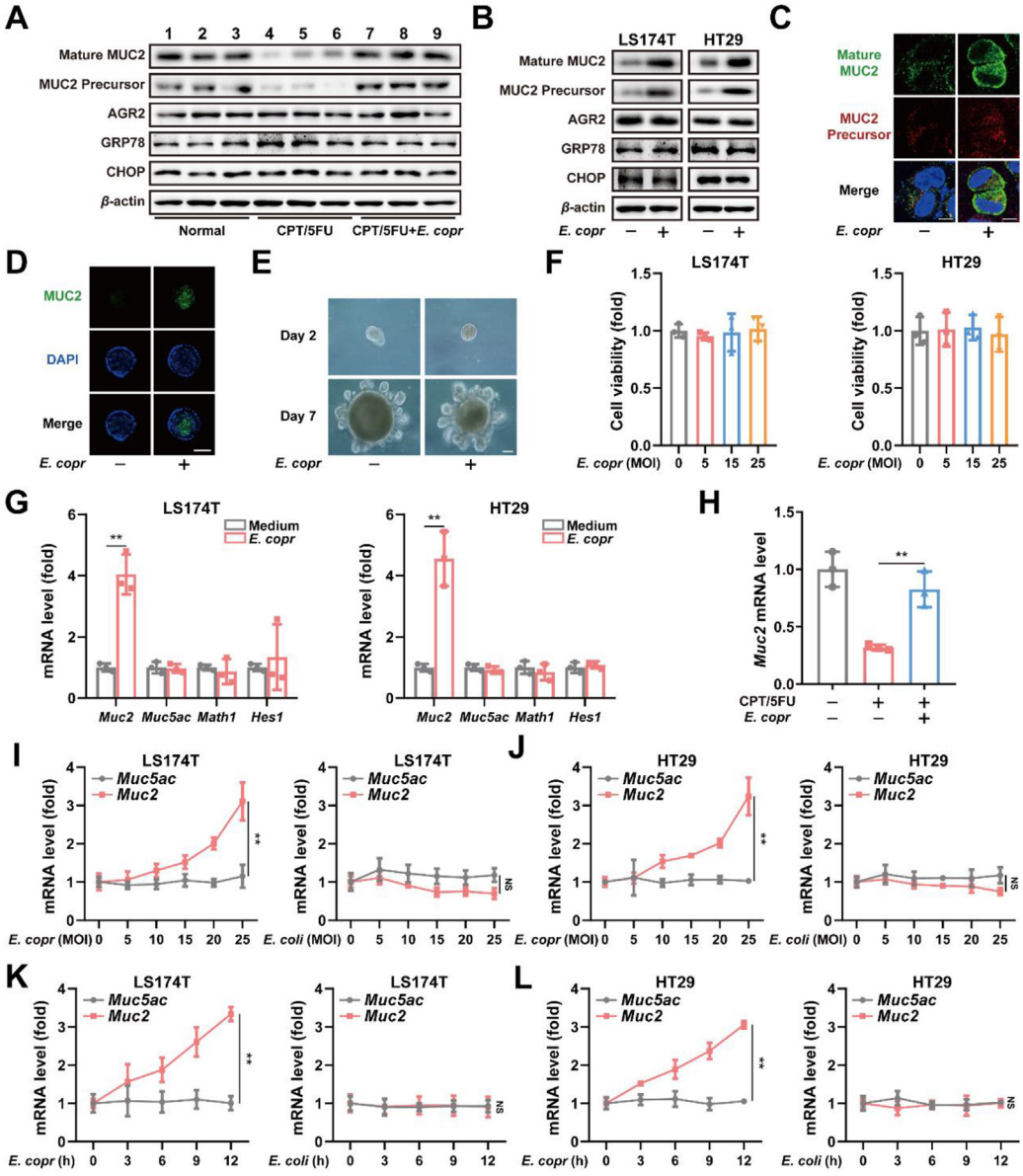

Figure 5 *E. copr* increased *Muc2* mRNA level in goblet cells. (A) Expressions of mature MUC2, MUC2 precursor, AGR2, GRP78 and CHOP were analyzed by Western blot in colon tissues of mucositis mice. (B) Expressions of mature MUC2, MUC2 precursor, AGR2, GRP78 and CHOP were analyzed by Western blot in LS174T and HT29 cells. (C) Mature MUC2 and MUC2 precursor immunofluorescence staining were performed in LS174T cells. Scale bar: 10 μm. (D) Immunofluorescence staining of MUC2 were performed in intestinal organoids. Scale bar: 100 μm. (E) Light microscopy images were collected from intestinal organoids at passage 2. Scale bar: 100 μm. (F) Cell viability was measured in LS174T and HT29 cells infected with different amounts of *E. copr*. (G) The mRNA levels of *Muc2*, *Muc5ac*, *Math1* and *Hes1* were measured in LS174T and HT29 cells infected with *E. copr* (MOI = 25). (H) The mRNA level of *Muc2* was measured in the colon tissues of indicated group mice. The mRNA levels of *Muc2* and *Muc5ac* were measured in LS174T (I) and HT29 (J) cells infected with different amounts of *E. copr* or *E. coli*. The mRNA levels of *Muc2* and *Muc5ac* were measured in LS174T (K) and HT29 (L) cells infected with *E. copr* (MOI = 25) or *E. coli* (MOI = 25) for different time. The values are expressed as the mean ± SD, $^{**}P < 0.01$. NS, not significant.

between RNA Pol-II and *Auf1* promoter was AhR dependent, as AhR knockdown blocked the interaction between RNA pol-II and AUF1 promoter (Fig. 7I).

Next, we sought to determine whether AhR is involved in *E. copr*-mediated upregulation of *Auf1* mRNA. As shown in Fig. 7J and K, *E. copr* infection led to a significant increase in *Auf1* mRNA levels, which was abolished after AhR knockdown. Furthermore, the upregulation of *Muc2* protein and mRNA expression induced by *E. copr* was also abolished in AhR knockdown cells (Fig. 7L and M). These findings indicate that *E. copr* promotes *Auf1* transcription and stabilizes *Muc2* mRNA through AhR activation.

3.8. E. copr alleviates CPT and 5FU induced intestinal mucositis by activating AhR

To investigate the role of the AhR in *E. copr*-mediated alleviation of chemotherapy-induced intestinal mucositis, we treated intestinal mucositis model mice with *E. copr* and the AhR inhibitor CH223191. Monitoring the mice's body weight, we observed that *E. copr* mitigated the weight loss induced by chemotherapy. However, this effect was significantly blocked by CH223191 treatment (Fig. 8A). Moreover, *E. copr* effectively inhibited chemotherapy-induced colon shortening, a response that was subsequently reversed by CH223191 treatment (Fig. 8B and C). Likewise, *E. copr* mitigated colonic tissue damage and suppressed the generation and release of inflammatory factors induced by chemotherapy. However, this protective effect was abrogated by CH223191 treatment (Fig. 8D−F). Additionally, we observed that *E. copr* played a crucial role in restoring the mouse colonic mucous layer and promoting MUC2 secretion. However, these beneficial effects were abolished upon treatment of CH223191 (Fig. 8G−I). In conclusion, our results collectively demonstrate that *E. copr* alleviates chemotherapy-induced intestinal mucositis through the activation of AhR.

4. Discussion

The intestinal mucosal barrier, predominantly composed of intestinal epithelial cells and the overlaying mucus layer, serves as a vital defense mechanism against microbial invasion. However, chemotherapy, while exerting its anticancer effects, also inflicts damage to intestinal epithelial cells, leading to intestinal mucositis. Previous research has predominantly focused on mitigating chemotherapy-induced intestinal epithelial cell injury to treat mucositis. Nevertheless, the pathogenesis of mucositis extends beyond mere intestinal epithelial cell damage; it also involves the thinning or loss of the mucus layer, thereby facilitating microbial infiltration. Microbial invasion triggers intense inflammatory responses, culminating in further damage to intestinal epithelial cells, perpetuating a vicious cycle that eventually results in mucositis. Therefore, targeting specific processes within this cascade could relieve intestinal mucositis. Our study reveals that *E. copr* recovers MUC2 expression following chemotherapy-induced loss of colonic mucus, thus ameliorating mucositis. Mechanistic investigations confirm that *E. copr* achieves this effect by activating AhR, thereby promoting AUF1 expression, which subsequently stabilizes *Muc2* mRNA. Consequently, *E. copr* holds promising potential as a novel therapeutic strategy for intestinal mucositis.

In order to evaluate the therapeutic effect of *E. copr* on chemotherapy-induced intestinal mucositis, it was essential to assess whether *E. copr* influences the anti-tumor efficacy of chemotherapeutic agents. By measuring tumor volume, tumor weight, cell proliferation and apoptosis levels, as well as the growth of orthotopic transplanted tumors in the colon, it was found that *E. copr* did not affect the anti-tumor activities of CPT and 5FU. Further investigations were performed on tumor-bearing mice, where we analyzed body weight, colon length, and colonic tissue histopathology to assess the impact of *E. copr* on chemotherapy-induced intestinal mucositis. Remarkably, *E. copr* demonstrated an ameliorating effect on chemotherapy-induced intestinal mucositis. Notably, despite maintaining colonic tissue integrity, *E. copr* did not influence apoptosis levels in colonic tissue. These observations were consistent in C57BL/6J mice as well. Thus, *E. copr* alleviates chemotherapy-induced intestinal mucositis without interfering with the pro-apoptotic effects of chemotherapeutic agents. Given the established role of gut microbiota and their metabolites in the formation of the mucus barrier, we hypothesized that *E. copr* might regulate the formation of this protective layer. To explore this, Alcian blue and PAS staining were performed, revealing that *E. copr* significantly restored the loss of colonic mucous layer induced by chemotherapy. This restoration was further supported by evaluating MUC2 expression. However, it is worth noting that *E. copr* did not affect chemotherapy-induced disruption of colonic tight junctions. Thus, the amelioration of chemotherapy-induced intestinal mucositis by *E. copr* does not result from the repair of the intestinal epithelial barrier, but rather from the restoration of the colonic mucus layer.

In the colon, MUC2 functions as the principal secreted mucin and undergoes a multifaceted process of synthesis and secretion. Following transcription and translation, MUC2 is synthesized as a precursor, which subsequently undergoes folding and glycosylation within the endoplasmic reticulum, culminating in the formation of mature MUC2. The mature MUC2 then undergoes sialylation modification, leading to the generation of a gel-like mucus that plays a crucial role in the formation of the mucus layer. While it has been observed that *E. copr* promotes the recovery of the colonic mucus layer, the specific mechanism underlying its influence on MUC2 production remains unclear. To address this, we initially evaluated the expression of mature MUC2, MUC2 precursor, and endoplasmic reticulum stress proteins. The results revealed that *E. copr* not only restored the mature MUC2 expression but also increased the MUC2 precursor expression, without affecting the endoplasmic reticulum stress proteins. These findings suggest that *E. copr* may not regulate the maturation process of MUC2 but rather directly influences its expression. Furthermore, qPCR results confirmed that *E. copr* treatment leads to elevated *Muc2* mRNA levels.

The upregulation of *Muc2* mRNA levels suggests that *E. copr* may promote both *Muc2* transcription and post-transcriptional modification. To elucidate the precise mechanism, we performed transcriptome sequencing and observed that the gene set involved in *Muc2* transcription activation was not significantly enriched. However, AUF1, an essential RNA-binding protein, exhibited a significant enrichment in the gene set associated with mRNA binding. Based on the results indicating an increased *Muc2* mRNA half-life upon treating of *E. copr*, we hypothesize that the upregulation of *Muc2* mRNA may rely on AUF1-mediated post-transcriptional modification. Previous studies have confirmed that AUF1 interacts with AREs to regulate mRNA stability. Consequently, we identified an ARE site within the 3′UTR of *Muc2* mRNA. By using truncation and point mutation approaches, we confirmed the binding of AUF1 to the ARE site in *Muc2* mRNA 3′UTR. The role of AUF1 in regulating mRNA stability can vary among different genes, stabilizing some mRNAs while degrading others. In our investigation, we observed that AUF1 stabilizes *Muc2* mRNA in goblet cells, and the increase of *E. copr*-induced *Muc2* mRNA depends on AUF1 expression.

Our findings not only provide confirmation that *E. copr* enhances the expression of *Muc2* mRNA dependent on AUF1, but also reveal an upregulation of both *Auf1* protein and mRNA levels by *E. copr*. Furthermore, we observed a significant reversal of the upregulated *Auf1* mRNA upon treatment with actinomycin D, leading to the complete abrogation of *de novo* transcription. These results strongly suggest that *E. copr* may play a key role in

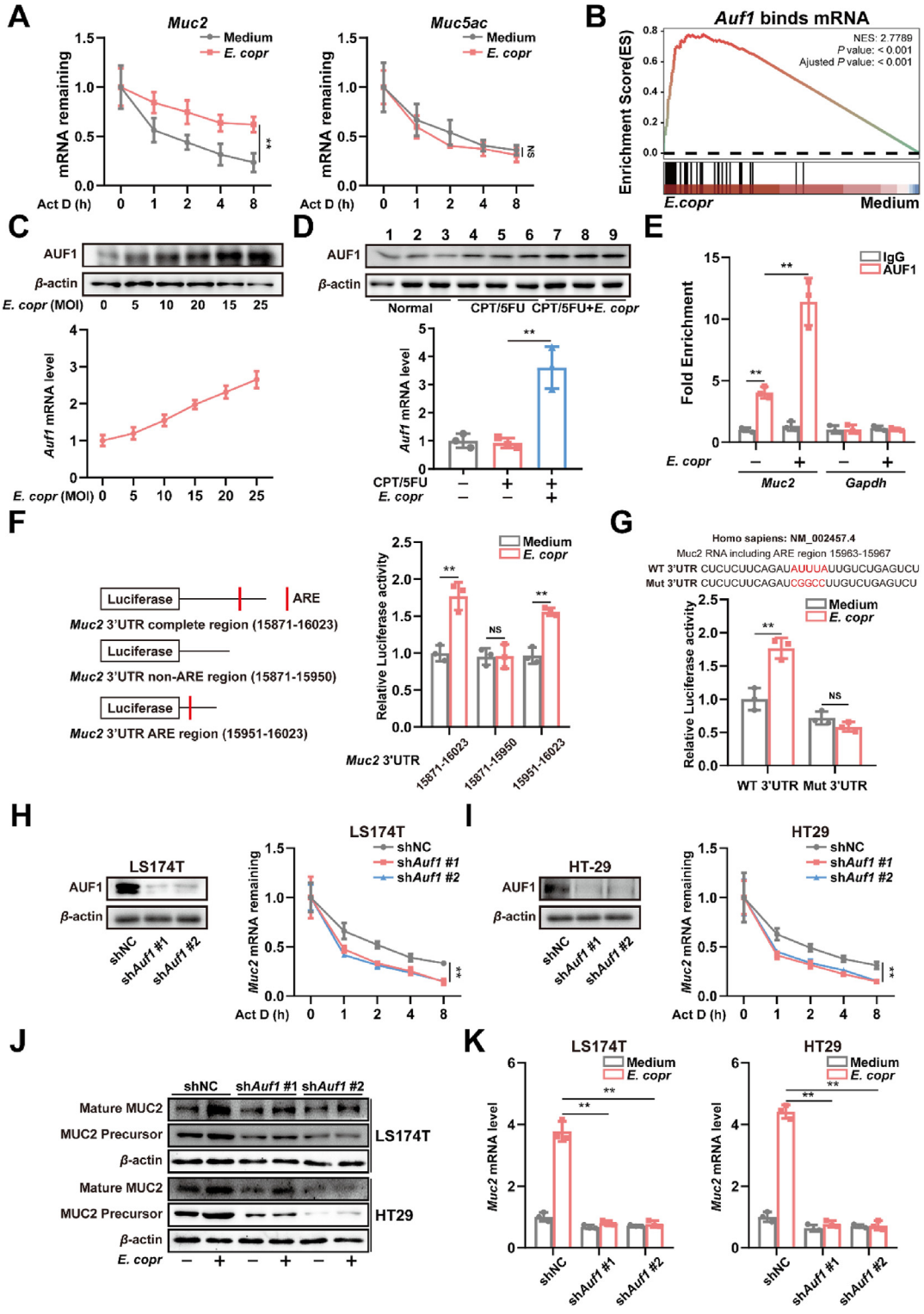

Figure 6 *E. copr* increased *Muc2* mRNA stability through AUF1. (A) After treatment with 5 μg/mL actinomycin D, total RNA was extracted at 0, 1, 2, 4, and 8 h. The half-lives of *Muc2* and *Muc5ac* mRNA were measured after infection with *E. copr* (MOI = 25). (B) GSEA analyses of Auf1 binds mRNA gene sets in LS174T cells treated with *E. copr vs* medium. (C) Expression of *Auf1* in protein (top) and mRNA (bottom) levels were analyzed in LS174T cells infected with different amounts of *E. copr*. (D) Expression of *Auf1* in protein (top) and mRNA (bottom) levels were analyzed in the colon tissues of indicated group mice. (E) *Muc2* mRNA expression was measured by qPCR in the RNA-binding protein immunoprecipitation (RIP) assay, and normalized to IgG isotype controls. (F) Diagram of the region of the pGL3 vector that encodes *Muc2* 3′UTR complete region (15871−16023), *Muc2* 3′UTR non-ARE region (15871−15950), or *Muc2* 3′UTR ARE region (15951−16023). The red bar shows the locations of AREs (left). The luciferase activities of each of the vectors encoding one of three different fragments of the *Muc2* 3′UTR were measured after infection with *E. copr* (MOI = 25) (right). (G) A predicted ARE region in the *Muc2* 3′UTR is shown in red (top). The luciferase

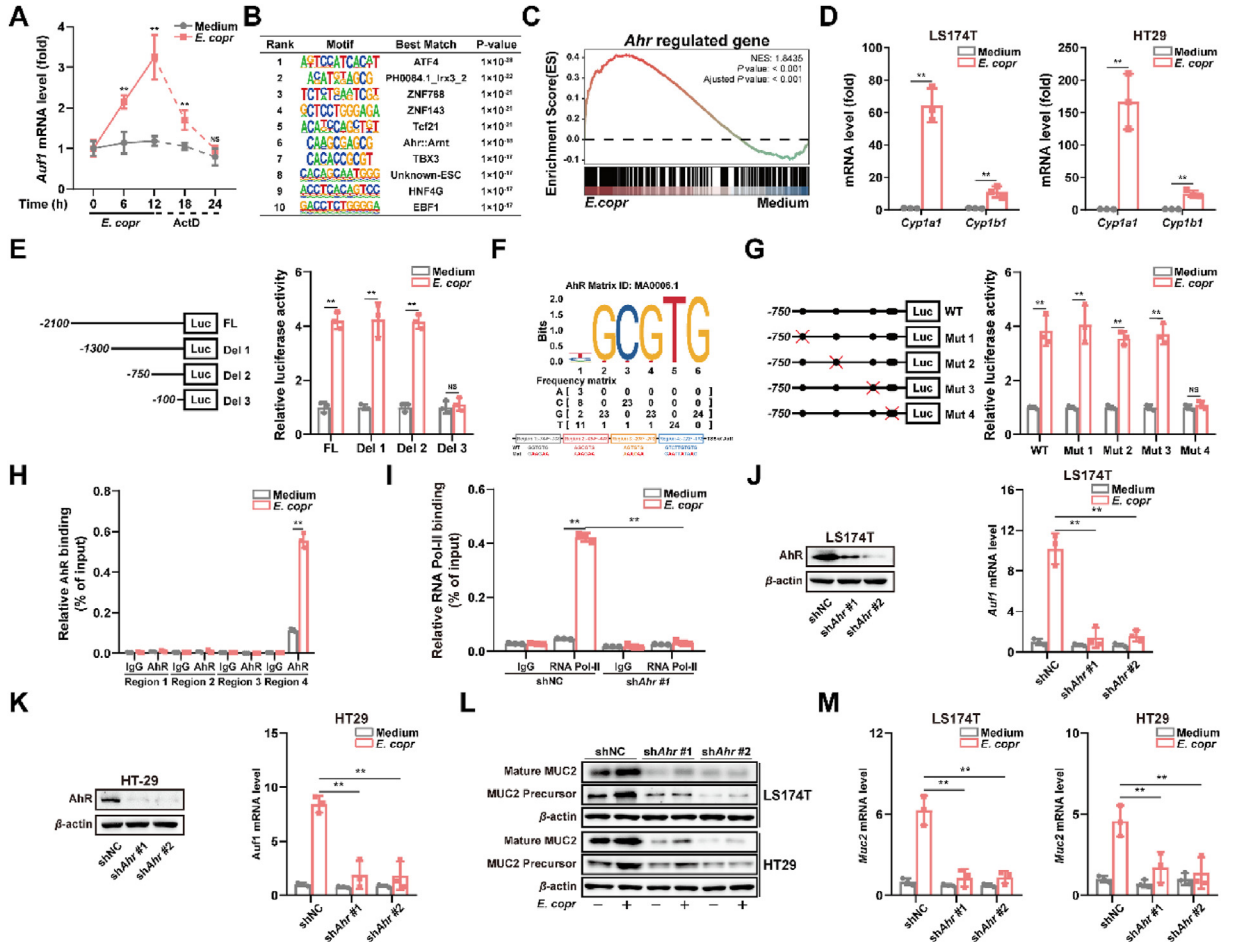

Figure 7 *E. copr* increased AUF1 transcription and *Muc2* mRNA stability through activating AhR. (A) After 12 h of infection with *E. copr* and another 12 h of treatment with actinomycin D, the *Auf1* mRNA levels were measured at specific times. (B) TF-binding site motif analysis for upregulated *Auf1* in LS174T cells. (C) GSEA analyses of AhR regulated gene sets in LS174T cells treated with *E. copr vs* medium. (D) The mRNA levels of *Cyp1a1* and *Cyp1b1* were measured in LS174T and HT29 cells after infection of *E. copr* (MOI = 25). (E) Schematic representation of the different luciferase reporter vectors of the 5′ deletions *Auf1* promoter (left). The luciferase activities of different 5′ deletions *Auf1* promoter were measured after infection of *E. copr* (MOI = 25) (right). (F) Sequence logo of AhR complement (top). Schematic representation of the different luciferase reporter vectors of the *Auf1* promoter mutants (bottom). (G) Schematic representation of the different luciferase reporter vectors of the 5′ mutation *Auf1* promoter (left). The luciferase activities of different 5′ mutation *Auf1* promoter were measured after infection with *E. copr* (MOI = 25) (right). (H) Chromatin from LS174T cells treated with *E. copr* or medium was analyzed for recruitment of AhR to the regulatory region of the *Auf1* promoter by ChIP-qPCR. (I) Chromatin from LS174T cells expressing *Ahr* shRNA after treatment of *E. copr* or medium was analyzed for recruitment of RNA Pol-II to the regulatory region of the *Auf1* promoter by ChIP-qPCR. The mRNA levels of *Auf1* were measured in LS174T (J) and HT29 (K) cells expressing *Ahr* shRNA after infection of *E. copr* (MOI = 25). (L) Expressions of mature MUC2 and MUC2 precursor were analyzed by Western blot in LS174T and HT29 cells expressing *Ahr* shRNA after infection of *E. copr* (MOI = 25). (M) The mRNA levels of *Muc2* were measured in LS174T and HT29 cells expressing *Ahr* shRNA after infection of *E. copr* (MOI = 25).

promoting the transcription of *Auf1*. The transcription relies on the binding of transcription factors to specific promoters. To identify the enriched TF binding motifs in *Auf1* promoter, we employed the HOMER algorithm. Our analysis revealed multiple significantly enriched TF binding motifs. Additionally, through GSEA using transcriptome sequencing data, we found evidence suggesting that AhR may be involved in the transcription of *Auf1*. Furthermore, we identified several putative AhR binding motifs in *Auf1* 5′UTR. To validate the role of *E. copr* in facilitating the binding of AhR to the *Auf1* promoter, we conducted a mutational analysis of the *Auf1* 5′UTR. Subsequently, we generated AhR knockdown cells and verified that the *E. copr*-induced transcription of *Auf1* and stabilization of *Muc2* mRNA depend on AhR expression.

Our study offers compelling evidence demonstrating the potential of *E. copr* to alleviate chemotherapy-induced intestinal

activities of each of the vectors encoding WT or mutant fragments of the *Muc2* 3′UTR were measured after infection with *E. copr* (MOI = 25) (bottom). The half-lives of *Muc2* mRNA were measured in LS174T (H) and HT29 (I) cells expressing *Auf1* shRNA. (J) Expressions of mature MUC2 and MUC2 precursor were analyzed by Western blot in LS174T and HT29 cells expressing *Auf1* shRNA after infection of *E. copr* (MOI = 25). (K) The mRNA levels of *Muc2* were measured in LS174T and HT29 cells expressing *Auf1* shRNA after infection of *E. copr* (MOI = 25).

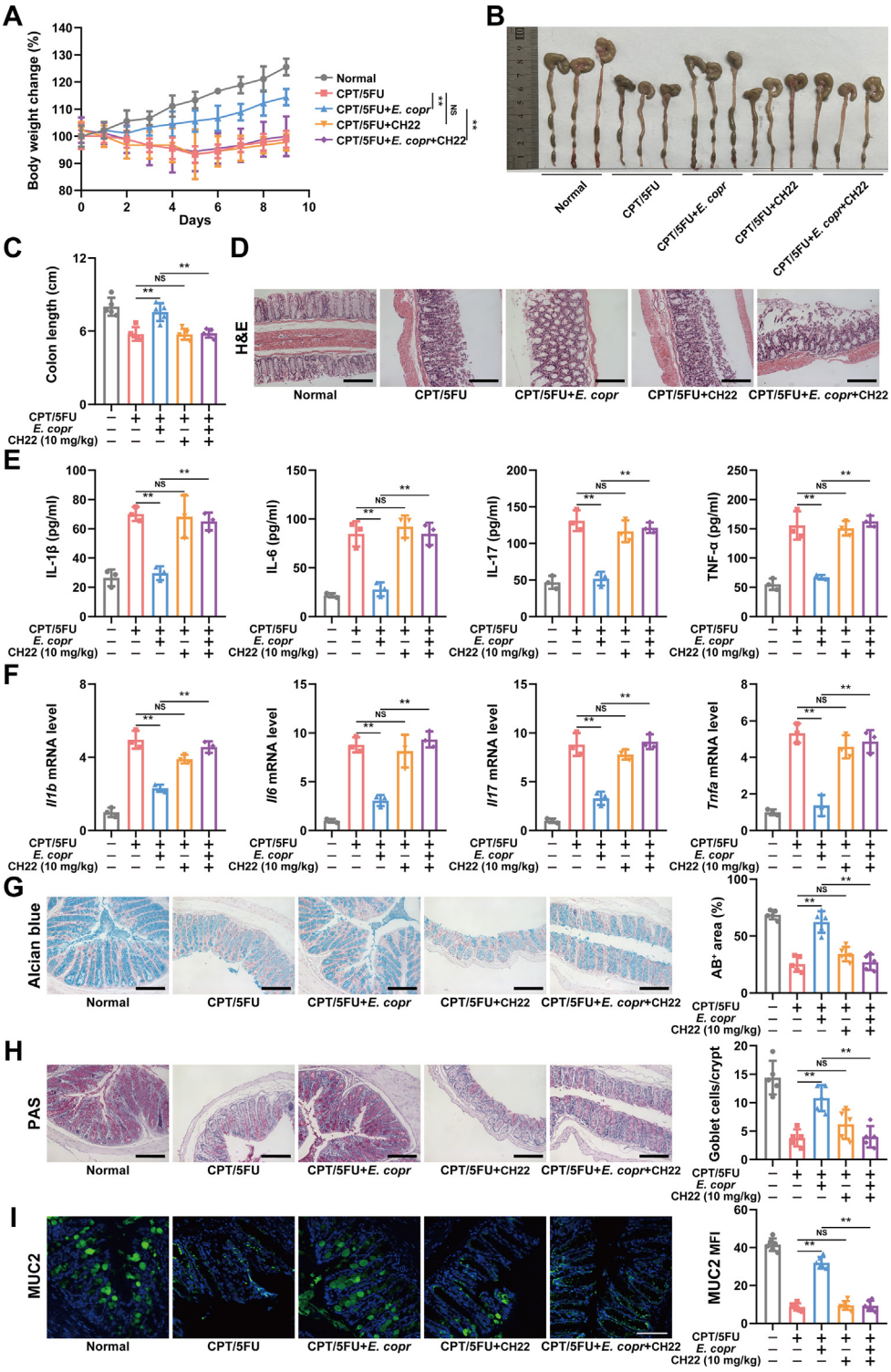

Figure 8 *E. copr* alleviated intestinal mucositis through activating AhR. (A) Body weight in the control, CPT/5FU, *E. copr*, CH223191 and the combination of *E. copr* and CH223191 groups were recorded daily. (B) Images of the colon in the indicated group were obtained on Day 9. (C) The colon length was measured in the indicated. (D) Representative images of the histopathology of the colon sections were obtained from indicated group. Scale bar: 100 μm. (E) Serum levels of IL-1β, IL-6, IL-17 and TNF-α were measured in the indicated group mice. (F) The mRNA levels of *Il1b*, *Il6*, *Il17* and *Tnfa* were measured in the colon tissues of indicated group mice. Alcian blue (G) and periodic acid-Schiff (H) were performed in colon sections of mucositis mice. Scale bar: 100 μm. (I) Expression of MUC2 was analyzed in colon sections of mucositis mice by immunofluorescence staining. Scale bar: 20 μm.

mucositis. Moreover, our findings emphasize the crucial role of intestinal mucus secretion, which is mediated by MUC2, in effectively defending against microbial invasion. Additionally, our research elucidates the role of AhR in regulating AUF1 expression, which stabilizes *Muc2* mRNA, by *E. copr*. However, it is essential to acknowledge that our mechanistic studies were conducted *in vitro* using cell lines, necessitating further investigations *in vivo*.

Acknowledgments

This work was supported by the National Natural Science Foundation of China (No. 82373910, 82204409). The "Double First-Class" University Project (CPU2022QZ20, China). We thank Mrs. Liuyi Zhong from Pharmaceutical Animal Experimental Center in China Pharmaceutical University for her kind help in the *in vivo* experiments.

Author contributions

Yue Zhao and Na Lu conceived and supervised the project. Dongsheng Bai, Jiawei Zhao, Runde Wang, Jiaying Du, Chen Zhou, Chunyang Gu and Yuxiang Wang performed experiments. Dongsheng Bai, Jiawei Zhao and Lulu Zhang are involved in acquisition of data, analysis and interpretation of data. Yue Zhao, Dongsheng Bai, Jiawei Zhao and Runde Wang analyzed the data and wrote the manuscript. All of the authors have read and approved the final manuscript.

Conflicts of interest

The authors have no conflicts of interest to declare.

References

1. Akbarali HI, Muchhala KH, Jessup DK, Cheatham S. Chemotherapy induced gastrointestinal toxicities. *Adv Cancer Res* 2022;**155**:131−66.
2. Wei L, Wen XS, Xian CJ. Chemotherapy-induced intestinal microbiota dysbiosis impairs mucosal homeostasis by modulating Toll-like receptor signaling pathways. *Int J Mol Sci* 2021;**22**:9474.
3. Docimo R, Anastasio MD, Bensi C. Chemotherapy-induced oral mucositis in children and adolescents: a systematic review. *Eur Arch Paediatr Dent* 2022;**23**:501−11.
4. De Pietri S, Weischendorff S, Rathe M, Frandsen TL, Hasle H, Nersting J, et al. Gastrointestinal barrier integrity and mucosal inflammation as risk factors of blood stream infections in children treated for acute lymphoblastic leukaemia. *Int J Cancer* 2023;**153**:1635−42.
5. Hino S, Yamada M, Iijima Y, Fujita Y, Sano M, Kaneko T, et al. Cancer chemotherapy-induced oral adverse events: oral dysesthesia and toothache−a retrospective study. *Ann Maxillofac Surg* 2021;**11**:86−90.
6. Wisinski K, Benson 3rd A. Chemotherapy-induced mucositis: focusing on diarrhea. *J Support Oncol* 2007;**5**:270−1.
7. Karthikeyan K, Babu CM, Shaji S, Ashok AM, Madhu CS. Case report on 5-fluorouracil induced cerebrovascular accident. *J Oncol Pharm Pract* 2021;**27**:1016−9.
8. Forsgard RA, Marrachelli VG, Korpela K, Frias R, Collado MC, Korpela R, et al. Chemotherapy-induced gastrointestinal toxicity is associated with changes in serum and urine metabolome and fecal microbiota in male Sprague−Dawley rats. *Cancer Chemother Pharmacol* 2017;**80**:317−32.
9. Calvo E, Cortes J, Gonzalez-Cao M, Rodriguez J, Aramendia JM, Fernandez-Hidalgo O, et al. Combined irinotecan, oxaliplatin and 5-fluorouracil in patients with advanced colorectal cancer. a feasibility pilot study. *Oncology* 2002;**63**:254−65.
10. Sobrero A, Guglielmi A, Cirillo M, Recaldin E, Frassineti GL, Aschele C, et al. 5-Fluorouracil modulated by leucovorin, methotrexate and mitomycin: highly effective, low-cost chemotherapy for advanced colorectal cancer. *Br J Cancer* 2001;**84**:1023−8.
11. McQuade RM, Al Thaalibi M, Nurgali K. Impact of chemotherapy-induced enteric nervous system toxicity on gastrointestinal mucositis. *Curr Opin Support Palliat Care* 2020;**14**:293−300.
12. Ribeiro RA, Wanderley CW, Wong DV, Mota JM, Leite CA, Souza MH, et al. Irinotecan- and 5-fluorouracil-induced intestinal mucositis: insights into pathogenesis and therapeutic perspectives. *Cancer Chemother Pharmacol* 2016;**78**:881−93.
13. Huang J, Hwang AYM, Jia Y, Kim B, Iskandar M, Mohammed AI, et al. Experimental chemotherapy-induced mucositis: a scoping review guiding the design of suitable preclinical models. *Int J Mol Sci* 2022;**23**:15434.
14. Oncel S, Basson MD. Gut homeostasis, injury, and healing: new therapeutic targets. *World J Gastroenterol* 2022;**28**:1725−50.
15. Tanes C, Walker EM, Slisarenko N, Gerrets GL, Grasperge BF, Qin X, et al. Gut microbiome changes associated with epithelial barrier damage and systemic inflammation during antiretroviral therapy of chronic SIV infection. *Viruses* 2021;**13**:1567.
16. Pandey P, Khan F. Gut microbiome in cancer immunotherapy: current trends, translational challenges and future possibilities. *Biochim Biophys Acta Gen Subj* 2023;**1867**:130401.
17. Yu J, Liu T, Gao Z, Liu R, Wang Z, Chen Y, et al. Akkermansia muciniphila colonization alleviating high fructose and restraint stress-induced jejunal mucosal barrier disruption. *Nutrients* 2022;**14**:3164.
18. Desai MS, Seekatz AM, Koropatkin NM, Kamada N, Hickey CA, Wolter M, et al. A dietary fiber-deprived gut microbiota degrades the colonic mucus barrier and enhances pathogen susceptibility. *Cell* 2016;**167**:1339−1353 e21.
19. Huang Z, Wu H, Fan J, Mei Q, Fu Y, Yin N, et al. Colonic mucin-2 attenuates acute necrotizing pancreatitis in rats by modulating intestinal homeostasis. *FASEB J* 2023;**37**:e22994.
20. Li XJ, Li Y, Meng Y, Pu XQ, Qin JW, Xie R, et al. Composite dissolvable microneedle patch for therapy of oral mucosal diseases. *Biomater Adv* 2022;**139**:213001.
21. Fernandez-Tome S, Ortega Moreno L, Chaparro M, Gisbert JP. Gut microbiota and dietary factors as modulators of the mucus layer in inflammatory bowel disease. *Int J Mol Sci* 2021;**22**:10224.
22. Huang X, Gao Y, Li S, Wu C, Wang J, Zheng N. Modulation of mucin (MUC2, MUC5AC and MUC5B) mRNA expression and protein production and secretion in Caco-2/HT29-MTX co-cultures following exposure to individual and combined aflatoxin M1 and ochratoxin A. *Toxins (Basel)* 2019;**11**:132.
23. Zarepour M, Bhullar K, Montero M, Ma C, Huang T, Velcich A, et al. The mucin Muc2 limits pathogen burdens and epithelial barrier dysfunction during *Salmonella enterica* serovar *Typhimurium colitis*. *Infect Immun* 2013;**81**:3672−83.
24. Niv Y. Mucin gene expression in the intestine of ulcerative colitis patients: a systematic review and meta-analysis. *Eur J Gastroenterol Hepatol* 2016;**28**:1241−5.
25. Xia B, Zhong R, Wu W, Luo C, Meng Q, Gao Q, et al. Mucin *O*-glycan-microbiota axis orchestrates gut homeostasis in a diarrheal pig model. *Microbiome* 2022;**10**:139.
26. Zhang Y, Wang L, Ocansey DKW, Wang B, Wang L, Xu Z. Mucin-type *O*-glycans: barrier, microbiota, and immune anchors in inflammatory bowel disease. *J Inflamm Res* 2021;**14**:5939−53.
27. Leon-Coria A, Kumar M, Workentine M, Moreau F, Surette M, Chadee K. Muc2 mucin and nonmucin microbiota confer distinct innate host defense in disease susceptibility and colonic injury. *Cell Mol Gastroenterol Hepatol* 2021;**11**:77−98.
28. Alarfaj SJ, Mostafa SA, Negm WA, El-Masry TA, Kamal M, Elsaeed M, et al. Mucosal genes expression in inflammatory bowel disease patients: new insights. *Pharmaceuticals (Basel)* 2023;**16**:324.

29. Bets VD, Achasova KM, Borisova MA, Kozhevnikova EN, Litvinova EA. Role of mucin 2 glycoprotein and L-fucose in interaction of immunity and microbiome within the experimental model of inflammatory bowel disease. *Biochemistry (Mosc)* 2022;**87**:301−18.
30. Arike L, Holmen-Larsson J, Hansson GC. Intestinal Muc2 mucin *O*-glycosylation is affected by microbiota and regulated by differential expression of glycosyltranferases. *Glycobiology* 2017;**27**:318−28.
31. Bai D, Sun T, Zhao J, Du J, Bu X, Cao W, et al. Oroxylin A maintains the colonic mucus barrier to reduce disease susceptibility by reconstituting a dietary fiber-deprived gut microbiota. *Cancer Lett* 2021;**515**:73−85.
32. Zhao Y, Guo Q, Zhao K, Zhou Y, Li W, Pan C, et al. Small molecule GL-V9 protects against colitis-associated colorectal cancer by limiting NLRP3 inflammasome through autophagy. *Oncoimmunology* 2017;**7**:e1375640.
33. Sato T, Vries RG, Snippert HJ, van de Wetering M, Barker N, Stange DE, et al. Single Lgr5 stem cells build crypt-villus structures without a mesenchymal niche. *Nature* 2009;**459**:262−5.
34. Jenvrin A, Perret A, Palmieri LJ, Soularue E, Broudin C, Rance B, et al. Chemotherapy-induced ileitis associated or not with colitis in digestive oncology patients: an AGEO multicentre study. *Dig Liver Dis* 2023;**55**:1426−33.
35. Sharpen JDA, Dolan B, Nystrom EEL, Birchenough GMH, Arike L, Martinez-Abad B, et al. Transglutaminase 3 crosslinks the secreted gel-forming mucus component Mucin-2 and stabilizes the colonic mucus layer. *Nat Commun* 2022;**13**:45.
36. Tawiah A, Moreau F, Kumar M, Tiwari S, Falguera J, Chadee K. High MUC2 mucin biosynthesis in goblet cells impedes restitution and wound healing by elevating endoplasmic reticulum stress and altered production of growth factors. *Am J Pathol* 2018;**188**:2025−41.
37. Yang L, Wang X, Zhao G, Deng L, Yin X. Leveraging temporal wnt signal for efficient differentiation of intestinal stem cells in an organoid model. *Stem Cells Dev* 2024;**33**:11−26.
38. He GW, Lin L, DeMartino J, Zheng X, Staliarova N, Dayton T, et al. Optimized human intestinal organoid model reveals interleukin-22-dependency of paneth cell formation. *Cell Stem Cell* 2022;**29**:1333−45.e6.
39. Yao X, Liu H, Wang Z, Lu F, Chen W, Feng Q, et al. Circular RNA EIF3I promotes papillary thyroid cancer progression by interacting with AUF1 to increase Cyclin D1 production. *Oncogene* 2023;**42**:3206−18.
40. Rajasekaran S, Khan E, Ching SR, Khan M, Siddiqui JK, Gradia DF, et al. PUMILIO competes with AUF1 to control DICER1 RNA levels and miRNA processing. *Nucleic Acids Res* 2022;**50**:7048−66.